

# Electric field induced gap modification in ultrathin blue phosphorous

Barun Ghosh,<sup>1</sup> Suhas Nahas,<sup>2</sup> Somnath Bhowmick,<sup>2,\*</sup> and Amit Agarwal<sup>1,†</sup>

<sup>1</sup>Department of Physics, Indian Institute of Technology, Kanpur 208016, India

<sup>2</sup>Dept. of Material Science and Engineering, Indian Institute of Technology, Kanpur 208016, India

(Dated: January 27, 2023)

Motivated by recent interest in various 2D crystals, we investigate the possibility of band structure engineering in the recently predicted blue phosphorous via a transverse electric field, using density functional theory based calculations. We consider both the monolayer and three differently stacked bilayer structures of blue phosphorous in presence of a transverse electric field and find that the default indirect bandgap becomes comparable to the direct band gap at the  $\Gamma$  point with increasing electric field ( $E_z \geq 0.4$  V/Å). Additionally, we also calculate the electron and hole effective masses along various symmetry directions in the reciprocal lattice. Our study may be useful to explore and optimize the potential application of monolayer and bilayer blue phosphorous in nanoelectronic and nanophotonic devices.

**Introduction:**— Various 2D crystals such as graphene<sup>1–3</sup>, silicene<sup>4–8</sup>, germanene<sup>5,9,10</sup>, transition metal dichalcogenides (MoS<sub>2</sub>, MoSe<sub>2</sub>, WSe<sub>2</sub> etc.)<sup>11,12</sup>, are being actively explored for the post Si nanoelectronics era, for their promise of aggressive channel length scalability on account of reduced short channel effects. Field effect transistors (FET's) based on graphene<sup>13</sup>, and MoS<sub>2</sub><sup>14</sup>, have already been demonstrated with performance which is superior to conventional Si based FET's. Layered black phosphorous (dubbed phosphorene) has joined this exciting family of 2D crystals of late, and FET's based on few layer black phosphorous have been fabricated with ON/OFF current ratio of  $\sim 10^5$ , and field effect mobility of  $\sim 1000$  cm<sup>2</sup>/Vs<sup>15–17</sup>.

More recently it has been predicted that, by certain dislocation of constituent P atoms, the puckered structure of black phosphorous (rectangular unit cell) can be converted to a more symmetric buckled structure (hexagonal unit cell) of another 2D allotrope, termed as the blue phosphorous<sup>18,19</sup>. The newly proposed allotrope is actually a single layer of the A7 phase of phosphorous<sup>20</sup>. Based on first principles calculations, a single layer of blue phosphorous is predicted to be as stable as monolayer black phosphorous<sup>18,19</sup>. Interestingly, electronic band structure of the two allotropes differ significantly. Unlike monolayer black phosphorous, which has an intrinsic direct bandgap of  $\sim 1.0$  eV at the  $\Gamma$  point, monolayer blue phosphorous has an indirect band gap of  $\sim 2$  eV<sup>18,19</sup>.

Bandgap engineering via stacking, applied strain or transverse electric field is essential for increasing the usefulness of various materials for applications in nanoelectronics and nanophotonics. A material with a tunable band gap, particularly by means of a transverse electric field, would allow for flexibility and optimization of its usage in various devices. The effect of transverse electric field on the band structure and electronic properties has earlier been studied both theoretically and experimentally for various 2D materials such as graphene<sup>21,22</sup>, silicene<sup>23,24</sup>, germanene<sup>24</sup>, transition metal dichalcogenides such as MoS<sub>2</sub><sup>25,26</sup>, black phosphorous<sup>27</sup> etc. As in the case of black phosphorous,

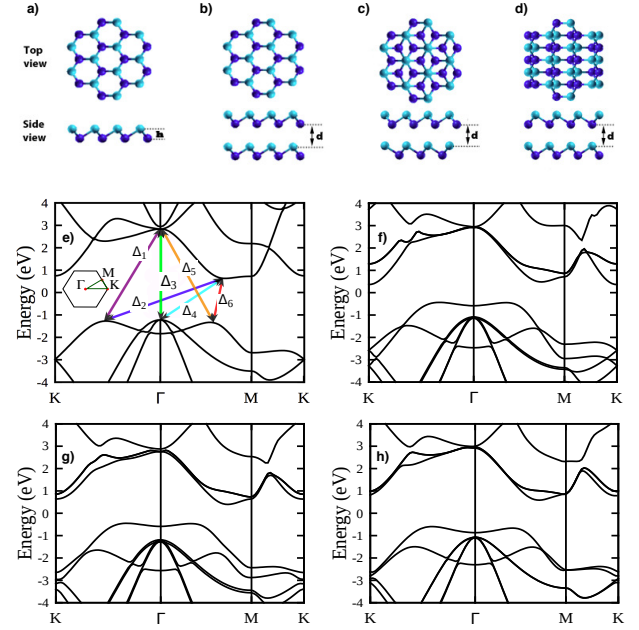


FIG. 1. Panels (a), (b), (c) and (d) display the layered structure and panels (e), (f), (g) and (h) show the electronic band structure of monolayer, AA, AB and AC stacked bilayer blue phosphorous, respectively. Atoms located at the top and bottom of the quasi-planar layers are distinguished by cyan and dark blue color, respectively and they form two interpenetrating hexagonal sublattices. The shaded area in (a)-(d) represents the unit cell. Panel (e) defines different energy gaps between valence and conduction band, whose electric field dependence is illustrated in Fig. 3. The intrinsic indirect bandgap is equal to  $\Delta_4$  in monolayer,  $\Delta_6$  in AA and AB stacked bilayer and  $\Delta_2$  in AC stacked bilayer blue phosphorous.

the band gap in blue phosphorous is expected to depend on the number of layers<sup>16</sup>, strain<sup>28</sup> and perpendicular applied electric field<sup>27</sup>. In this article we use *ab initio* density functional theory calculations to study the electric field induced gap modification in mono and bilayer

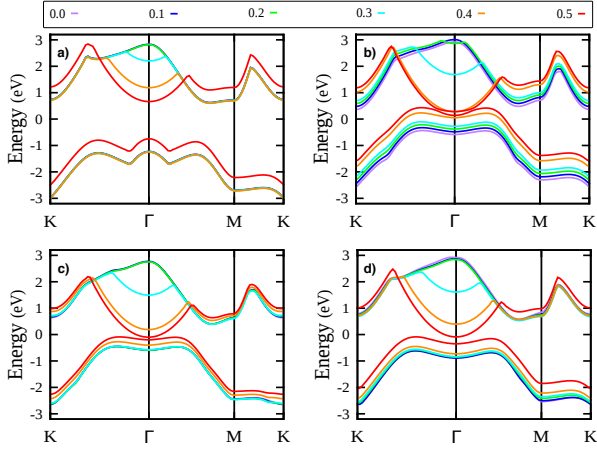


FIG. 2. Panels (a), (b), (c) and (d) study the effect of the transverse electric field on the lowest conduction band and highest valance band for monolayer, AA, AB and AC stacked bilayer blue phosphorus, respectively. Note that for all the four cases, the direct band gap at the  $\Gamma$  point [ $\Delta_3$ , as defined in Fig. 1(e)] decreases with increasing electric field, while the default indirect band gap almost remains constant. The transition from widegap indirect semiconductor to a narrow gap direct semiconductor and eventually to a metal with increasing electric field is evident in all four plots.

blue phosphorus considering three different stacking [see Fig. 1(a)-(d)].

*Computational Details:*— The *ab initio* calculations are performed by density functional theory (DFT), using a plane-wave basis set and ultrasoft pseudopotentials, as implemented in Quantum Espresso<sup>29</sup>. Electron exchange and correlation is treated within the framework of local density approximation (LDA), as well as generalized gradient approximation (GGA) for consistency check. Since the band diagrams obtained using LDA and GGA are found to be similar, only the LDA-based results are shown, unless stated otherwise. The kinetic energy cutoff for wave function is set to be 40 Ry. Supercell with a vacuum of 25 Å along the  $z$  direction (perpendicular to the blue phosphorous layers) is constructed to eliminate the interaction with spurious replica images. A  $k$ -point grid of  $24 \times 24 \times 1$  is used for the Brillouin zone integrations. Structural relaxations are carried out until the force on each atom (total energy change due to ionic relaxation between two successive steps) is less than  $10^{-3}$  Ry/au ( $10^{-4}$  Ry). An external sawtooth potential is used in the  $z$  direction to simulate the effect of an applied electric field perpendicular to the blue phosphorous layer(s).

*Results and discussions:*— The honeycomb net of P atoms in monolayer blue phosphorous is formed by two inter-penetrating hexagonal sublattices [shown in two different colors/shades in Fig. 1(a)]. However, unlike graphene and similar to silicene/germanene, the two sublattices in blue phosphorous are not in the same plane and the vertical distance between them is given by  $h$  [as shown Fig. 1(a),  $h = 1.24$  Å]. This results in a pseudo-

TABLE I. Equilibrium structural parameters for monolayer and differently stacked bilayer blue phosphorous.

Stacking	Bond length (Å)	Bond angle (Degree)	$d$ (Å)
Mono	2.23	90.84	-
AA	2.23	92.19	3.12
AB	2.24	92.31	3.06
AC	2.23	92.25	3.47

planar structure, where half of the atoms are buckled out of the plane, with P-P bond angle equal to 90.8°. Each of these monolayers can be stacked, so as to form multi layered structures in different ways, based on the relative displacement of the sublattices of one layer with respect to the other layers. In this paper, we consider bilayers stacked in three different sequences, namely AA [Fig. 1(b)], AB [Fig. 1(c)] and AC [Fig. 1(d)]. The unit cell has four atoms in total, two each in every layer. In case of AA stacking, the two sublattices belonging to each of the layers overlap directly and as a consequence, only two atoms per unit cell are visible in the top view [see Fig. 1(b)]. On the contrary, one constituent layer is displaced relative to the other one by a P-P bond length in case of AB stacking, such that one of the two sublattices of both the layers overlap directly and the other sublattice of the first layer is placed on top of the center of the honeycomb net of the second layer. Consequently, only three atoms per unit cell are visible in the top view of AB-stacked bilayer blue phosphorous, as shown in Fig. 1(c). Similar to AB, one layer of blue phosphorous is displaced with respect to the other one in case of AC stacking as well. However, unlike AB, none of the sublattices from the two layers are located directly on top of each other and thus, as illustrated in Fig. 1(d), all the four atoms per unit cell are visible in the top view. As reported in Table I, although the bond length and bond angle are nearly equal, irrespective of stacking sequence, the interplanar spacing  $d$  changes significantly; for example AC (maximum  $d$ ) has 10% more interplanar spacing than AB (minimum  $d$ ). Similarly, total energy of bilayer blue phosphorous also depends on the stacking sequence, AA being energetically the most favorable one, followed by AB and AC, having 2 meV/atom and 6 meV/atom higher energy than AA.

Electronic band structure is calculated along various high symmetry directions in the reciprocal lattice [see the inset of Fig. 1(e)] and the energy dispersion relations are shown in Fig. 1(e)-(h). As illustrated in the figure, we define six different values of energy gap between the valence and conduction band, namely  $\Delta_1$ ,  $\Delta_2$ ,  $\Delta_3$ ,  $\Delta_4$ ,  $\Delta_5$  and  $\Delta_6$  and among them  $\Delta_3$  is the only direct energy gap (measured at  $\Gamma$  point). The choice is made on the basis of the fact that, actual bandgap of mono or bilayer blue phosphorous in zero or finite electric field is equal to one of the  $\Delta_i$ 's, as defined in Fig. 1(e). For example, in zero electric field single layer of blue phos-

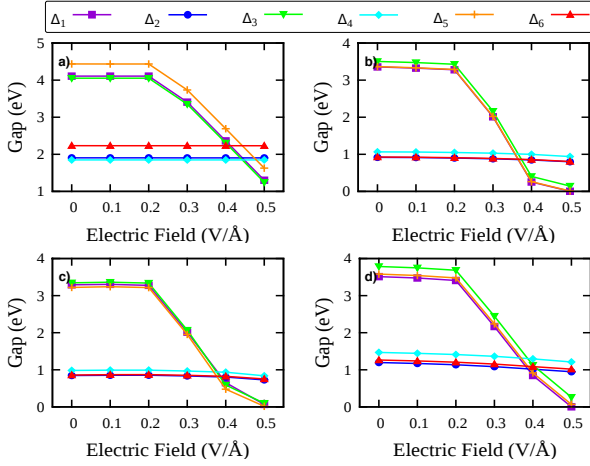


FIG. 3. Panels (a), (b), (c) and (d) study the effect of the transverse electric field on the various bandgaps specified in Fig. 1(e), for monolayer, AA, AB and AC stacked bilayer blue phosphorus, respectively. Note that  $\Delta_3$  (green triangle pointing downwards) denotes the direct bandgap at the  $\Gamma$  point, while all other  $\Delta$ 's represent indirect band-gaps. In all the panels, the direct bandgap at the  $\Gamma$  point decreases with increasing electric field, and becomes comparable to the indirect band gap, and both of which vanish for electric field strength of  $\sim 0.5$  V/Å, making blue phosphorous metallic.

phorous is an indirect bandgap semiconductor and the bandgap is equal to  $\Delta_4$  [see Fig. 1(e)]. The electronic band structure is qualitatively similar for both LDA and GGA based calculations, although the magnitude differ slightly; 1.85 eV (LDA) and 1.93 eV (GGA), respectively and the values compare well with those reported in the literature<sup>18</sup>. Similarly, bilayer blue phosphorous is also an indirect bandgap semiconductor and depending on the stacking sequence, the bandgap is equal to  $\Delta_6$  (AA and AB) or  $\Delta_2$  (AC), although  $\Delta_6 \sim \Delta_2$  for all three of them [see Fig. 1(f)-(h)]. Depending on the stacking sequence, the magnitude of the bandgap of bilayer blue phosphorous varies from 0.8 eV (AA) to 1.2 eV (AC), almost 40–50% less than that of monolayer blue phosphorous.

We now explore the effect of an externally applied transverse electric field on the electronic band structure of monolayer and bilayer blue phosphorous. For this purpose, an electric field is applied in a direction perpendicular to the blue phosphorous layer (ranging from 0.1 V/Å to 0.5 V/Å, in steps of 0.1 V/Å), which is similar to applying a gate voltage in FET's. We find that, unlike silicene<sup>24</sup>, electric field does not affect the buckling in case of blue phosphorous (value of  $h$  changes by 0.02% when the strength of electric field is increased from 0 to 0.5 V/Å) and other structural parameters like bond length and bond angle also do not change significantly. Although there is no considerable structural modification, but electronic band structure changes substantially, particularly at higher value of applied electric field [see Fig. 2(a) and Fig. 3(a)]. As shown in the figure, upto

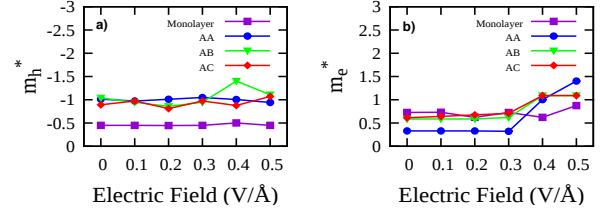


FIG. 4. Panels (a) and (b) display the variation of hole and electron effective mass at valence band maxima (VBM) and conduction band minima (CBM) for mono layer and differently stacked bilayer blue phosphorus. If the VBM or CBM occurs in the middle of  $\Gamma$ M or  $\Gamma$ K, the effective mass is calculated in that particular direction. Otherwise, at the  $\Gamma$  point, it is found to be isotropic.

0.2 V/Å the electronic band structure of monolayer blue phosphorous is mostly unaffected by the applied field and the change is readily apparent only when the applied field is 0.3 V/Å or more. Interestingly, the most significant change occurs at the conduction band edge at  $\Gamma$  point, which starts shifting towards the VBM (also at the  $\Gamma$  point) and as a result value of  $\Delta_1$ ,  $\Delta_3$  and  $\Delta_5$  decreases with increasing electric field, while  $\Delta_2$ ,  $\Delta_4$  and  $\Delta_6$  remains unchanged [see Fig. 3(a)]. As illustrated in Fig. 3(a), monolayer blue phosphorous remains indirect bandgap (magnitude equal to  $\Delta_4$ ) semiconductor upto 0.4 V/Å applied field. However, when the electric field is increased further to 0.5 V/Å, the downward shift of conduction band edge at  $\Gamma$  point is so large that the conduction band minima (CBM) is relocated to the  $\Gamma$  point (from its original position, in the middle of  $\Gamma$ M), converting monolayer blue phosphorous to a direct bandgap (magnitude equal to  $\Delta_3$ ) semiconductor [see Fig. 2(a) and Fig. 3(a)]. Note that, the valence band maxima does not change significantly even at higher electric field; although it shifts to close the bandgap at 0.5 V/Å applied field, valence band maxima (VBM) still remains located at the  $\Gamma$  point.

Similar to the monolayer, structural parameters of bilayer blue phosphorous, like bond length, bond angle and buckling ( $h$ ) is hardly affected by externally applied electric field and interplanar spacing changes only by 0.48% in AA, 1.14% in AB and 0.33% in AC, as the electric field increases from 0 to 0.5 V/Å. Like single layer of blue phosphorous, the most significant change to the electronic band structure also occurs at the conduction band edge at  $\Gamma$  point, which gradually shifts downward with increasing electric field, starting from 0.3 V/Å and higher [see Fig. 2(b)-(d)]. As a result, the conduction band minima, which is originally located approximately in the middle of  $\Gamma$ M, is shifted to the  $\Gamma$  point at 0.4 V/Å electric field [see Fig. 2(b)-(d)]. Consequently, the bandgap changes from  $\Delta_6$  to  $\Delta_5$  in AA and AB and from  $\Delta_2$  to  $\Delta_1$  in AC [see Fig. 3(b)-(d)]. Note that unlike monolayer, which changes from indirect to direct bandgap semiconductor at higher electric field, bilayer blue phosphorous

remains an indirect bandgap semiconductor. However the value of direct energy gap at  $\Gamma$  point,  $\Delta_3$ , is very close to the actual bandgap  $\Delta_1/\Delta_5$  for each of the bi-layer blue phosphorous.

Having discussed the effect of transverse electric field on the bandgap, we move on to the effective mass which determines the electron/hole mobility and thus also controls the transport properties. From the energy dispersion relation, the effective mass is calculated both at VBM ( $m_h^*$ ) and CBM ( $m_e^*$ ). As shown in Fig. 4(a), the effective mass of holes ( $m_h^*$ ) does not change significantly as a function of the transverse electric field, since the shape of the valance bands is not affected by the transverse electric field [see Fig. 2]. However, depending on the number of layers and stacking sequence  $m_e^*$  increases by a factor of 1.5 to 4 with increasing electric field [see Fig. 4(b)], which can be attributed to the shifting of CBM to  $\Gamma$  point from it's original location at zero or smaller electric field.

*Conclusion:*— To summarize, we have explicitly shown that monolayer and bilayers of blue phosphorous, are versatile new 2D materials, in which the band gap can be tuned from  $\sim 2$  eV ( $\sim 1$  eV) for monolayer (bilayer) to 0

eV, by means of a transverse electric field. Broadly, we find that, the default indirect band gap remains constant while the direct band gap at the  $\Gamma$  point, and another indirect band gap decreases (almost linearly) with increasing electric field. Both monolayer and bi-layer blue phosphorous undergo a transition from indirect band gap insulator to direct band gap insulator (for  $E_z \geq 0.4$  V/Å), and eventually to metal (for  $E_z \geq 0.5$  V/Å). All these changes in the band structure are also reflected in the effective mass. Finally, we note that in monolayer black phosphorene, a transverse electric field has no effect on the band structure and consequently on the intrinsic direct band gap or effective mass, as opposed to monolayer blue phosphorous discussed in this article, and this may be used as a probe to distinguish between the two.

## ACKNOWLEDGEMENTS

We acknowledge funding from the DST INSPIRE Faculty Award, DST Fasttrack Scheme for Young Scientist and the Faculty Initiation Grant by IIT Kanpur. We also thank CC IITK for providing HPC facility.

---

\* [bsomnath@iitk.ac.in](mailto:bsomnath@iitk.ac.in)

† [amitag@iitk.ac.in](mailto:amitag@iitk.ac.in)

- <sup>1</sup> A. K. Geim and K. S. Novoselov, *Nat. Mater.* **6**, 183 (2007)
- <sup>2</sup> A. H. Castro Neto, F. Guinea, N. M. R. Peres, K. S. Novoselov, and A. K. Geim, *Rev. Mod. Phys.* **81**, 109 (2009)
- <sup>3</sup> M. I. Katsnelson, *Graphene* (Cambridge University Press, 2012) cambridge Books Online
- <sup>4</sup> K. Takeda and K. Shiraishi, *Phys. Rev. B* **50**, 14916 (1994)
- <sup>5</sup> G. G. Guzmán-Verri and L. C. Lew Yan Voon, *Phys. Rev. B* **76**, 075131 (2007)
- <sup>6</sup> B. Lalmi, H. Oughaddou, H. Enriquez, A. Kara, S. Vizzini, B. Ealet, and B. Aufray, *Appl. Phys. Lett.* **97**, 223109 (2010)
- <sup>7</sup> P. Vogt, P. De Padova, C. Quaresima, J. Avila, E. Frantzeskakis, M. C. Asensio, A. Resta, B. Ealet, and G. Le Lay, *Phys. Rev. Lett.* **108**, 155501 (2012)
- <sup>8</sup> L. Chen, C.-C. Liu, B. Feng, X. He, P. Cheng, Z. Ding, S. Meng, Y. Yao, and K. Wu, *Phys. Rev. Lett.* **109**, 056804 (2012)
- <sup>9</sup> E. Bianco, S. Butler, S. Jiang, O. D. Restrepo, W. Windl, and J. E. Goldberger, *ACS Nano* **7**, 4414 (2013)
- <sup>10</sup> S. Cahangirov, M. Topsakal, E. Aktürk, H. Şahin, and S. Ciraci, *Phys. Rev. Lett.* **102**, 236804 (2009)
- <sup>11</sup> M. Chhowalla, H. S. Shin, G. Eda, L.-J. Li, K. P. Loh, and H. Zhang, *Nat. Chem.* **5**, 263 (2013)
- <sup>12</sup> X. Xu, W. Yao, D. Xiao, and T. F. Heinz, *Nature Phys.* **10**, 343 (2014)
- <sup>13</sup> F. Schwierz, *Nat. Nanotechnol.* **5**, 487 (2010)
- <sup>14</sup> B. Radisavljevic, R. A. B. J. G. V., and K. A., *Nat. Nanotechnol.* **6**, 147 (2011)

- <sup>15</sup> L. Li, Y. Yu, G. J. Ye, Q. Ge, X. Ou, H. Wu, D. Feng, X. H. Chen, and Y. Zhang, *Nat. Nanotechnol.* **9**, 372 (2014)
- <sup>16</sup> H. Liu, A. T. Neal, Z. Zhu, Z. Luo, X. Xu, D. Tománek, and P. D. Ye, *ACS Nano* **8**, 4033 (2014)
- <sup>17</sup> S. P. Koenig, R. A. Doganov, H. Schmidt, A. H. Castro Neto, and B. zylmaz, *Appl. Phys. Lett.* **104**, 103106 (2014)
- <sup>18</sup> Z. Zhu and D. Tománek, *Phys. Rev. Lett.* **112**, 176802 (2014)
- <sup>19</sup> J. Guan, Z. Zhu, and D. Tománek, *Phys. Rev. Lett.* **113**, 046804 (2014)
- <sup>20</sup> S. E. Boulfelfel, G. Seifert, Y. Grin, and S. Leoni, *Phys. Rev. B* **85**, 014110 (2012)
- <sup>21</sup> E. V. Castro, K. S. Novoselov, S. V. Morozov, N. M. R. Peres, J. M. B. L. dos Santos, J. Nilsson, F. Guinea, A. K. Geim, and A. H. C. Neto, *Phys. Rev. Lett.* **99**, 216802 (2007)
- <sup>22</sup> Y. Zhang, T.-T. Tang, C. Girit, Z. Hao, M. C. Martin, A. Zettl, M. F. Crommie, Y. R. Shen, and F. Wang, *Nature* **459**, 820 (2009)
- <sup>23</sup> N. D. Drummond, V. Zólyomi, and V. I. Fal'ko, *Phys. Rev. B* **85**, 075423 (2012)
- <sup>24</sup> Z. Ni, Q. Liu, K. Tang, J. Zheng, J. Zhou, R. Qin, Z. Gao, D. Yu, and J. Lu, *Nano Lett.* **12**, 113 (2012)
- <sup>25</sup> Q. Liu, L. Li, Y. Li, Z. Gao, Z. Chen, and J. Lu, *J. Phys. Chem. C* **116**, 21556 (2012)
- <sup>26</sup> A. Ramasubramaniam, D. Naveh, and E. Towe, *Phys. Rev. B* **84**, 205325 (2011)
- <sup>27</sup> J. Dai and X. C. Zeng, *J. Phys. Chem. Lett.* **5**, 1289 (2014)
- <sup>28</sup> A. S. Rodin, A. Carvalho, and A. H. Castro Neto, *Phys. Rev. Lett.* **112**, 176801 (2014)
- <sup>29</sup> P. Giannozzi, S. Baroni, N. Bonini, M. Calandra, *et al.*, *J. Phys.: Condens. Matter* **21**, 395502 (2009)